VNU Journal of Science: Mathematics - Physics

Journal homepage: https://js.vnu.edu.vn/MaP

Original Article

Two Dimensional Infinite Semi-parabolic Asymmetric Quantum Wells: Ettingshausen Coefficient under the Influence of Intense Electromagnetic Wave

Nguyen Thi Nguyet Anh[1,*], Nguyen Thu Huong[2], Nguyen Quang Son[2], Pham Tien Thanh[1]

[1] *VNU University of Science, 334 Nguyen Trai, Thanh Xuan, Hanoi, Vietnam*

[2] *Air Defence-Air Force Academy, Doai Phuong, Hanoi, Vietnam*

Received 14th October 2025

Revised 6th November 2025; Accepted 31st July 2026

Abstract: A theoretical study is presented for the quantum Ettingshausen effect in a two-dimensional electron gas confined by an infinite semi-parabolic asymmetric quantum well (ISPQW) and subjected to an intense electromagnetic wave (EMW). Within the framework of the quantum kinetic equation, we derive new analytical forms of the dynamic transport tensors (σ, β, γ, and ξ) together with the Ettingshausen coefficient (EC), explicitly incorporating electron–acoustic phonon scattering. Numerical evaluations for GaAs/AlGaAs heterostructures demonstrate that the EC strongly and nonlinearly depends on the magnetic field (B), temperature (T), EMW frequency (Ω), and confinement frequency (ω_z). The EC exhibits distinct Shubnikov–de Haas (SdH) quantum oscillations, whose amplitudes increase with temperature while their peak positions remain almost unchanged. Conversely, both stronger magnetic fields and higher EMW frequencies suppress these oscillations. Furthermore, variations with confinement frequency ω_z produce large-amplitude quantum oscillations, reflecting strong quantization effects arising from the asymmetric confining potential. These findings elucidate how structural asymmetry and electron–phonon coupling shape quantum thermomagnetic transport, offering valuable insights for the design of advanced low-dimensional thermoelectric systems.

Keywords: Ettingshausen effect, infinite semi-parabolic asymmetric quantum well (ISPQW), intense electromagnetic wave, quantum kinetic equation, electron–acoustic phonon scattering, Shubnikov–de Haas oscillation, quantum thermoelectric transport.

[*] Corresponding author.

E-mail address: anhntn.hsgs@hus.edu.vn

https//doi.org/10.25073/2588-1124/vnumap.5091

1. Introduction

The study of magneto-thermoelectric transport in two-dimensional electron gases (2DEGs) has provided profound insights into the fundamental physics of quantum-confined systems [1-3]. The Ettingshausen effect (EC), which manifests as a transverse temperature gradient induced by mutually perpendicular electric and magnetic fields, serves as a powerful probe of such quantum phenomena [1, 4]. Most theoretical investigations to date have concentrated on 2DEGs confined within symmetric potentials, particularly square and parabolic quantum wells [2, 5]. These foundational studies have established a comprehensive understanding of the EC behavior in idealized, symmetric environments, highlighting its strong dependence on scattering mechanisms and quantum confinement effects [3].

However, the vast majority of these works are limited to systems possessing spatial inversion symmetry [2, 5]. The influence of asymmetry in the confinement potential on magneto-thermoelectric transport remains a largely unexplored frontier. This gap in the literature is not trivial, as the underlying quantum mechanics of symmetric and asymmetric systems are fundamentally different. Breaking the potential's symmetry directly alters the system's core properties: the electron wave functions no longer possess definite parity, and the energy spectrum is significantly modified. These changes inevitably impact the matrix elements for carrier scattering and the selection rules for transitions, suggesting that transport coefficients like the Ettingshausen coefficient should exhibit qualitatively new behaviors [1, 6].

To address this, our work provides a foundational theoretical analysis of the Ettingshausen effect in a canonical asymmetric system: a 2DEG confined by an infinite semi-parabolic asymmetric quantum well (ISPQW). We focus on the transport regime dominated by electron-acoustic phonon scattering, a crucial interaction in semiconductor heterostructures. By employing the quantum kinetic equation, we derive an analytical expression for the Ettingshausen coefficient and systematically analyze its behavior as a function of temperature, magnetic field, and the characteristic confinement frequency.

The central goal of this paper is to elucidate how the inherent asymmetry of the semi-parabolic potential manifests in the magneto-thermoelectric response. By comparing our results to the established behaviors in symmetric wells, we aim to uncover the unique signatures of asymmetry in the EC, providing new insights into the engineering of thermal transport in nanostructures.

The paper is organized as follows: Sec. (2) details the theoretical model and analytical derivations. Sec. (3) presents and discusses the numerical results for a GaAs/AlGaAs-based ISPQW. Sec. (4) provides the concluding remarks.

2. Theoretical Framework

2.1. Stationary States of Electron in the Infinite Semi-parabolic Asymmetric Quantum Well

In this study, we examine the transport behavior of an electron gas confined within a quantum well heterostructure. The system is modeled such that the electron motion is quantized along the growth direction (z-axis) by an infinite semi-parabolic confinement potential $\mathcal{V}(z)$, while the electrons remain free to move in the transverse (x-y) plane [7]

$$\mathcal{V}(z) = \begin{cases} \infty, & \mathrm{z} < 0 \\ \mathcal{A}\mathrm{z}^2, & \mathrm{z} \geq 0 \end{cases}, \tag{1}$$

in which $\mathcal{A} = \frac{\mathrm{m_e}\omega_\mathrm{z}^2}{2}$, ω_z is the characteristic confinement frequency; $\mathrm{m_e} = 0.067\mathrm{m_0}$ is the effective mass of the electron, with $\mathrm{m_0}$ being the free electron rest mass.

A longitudinal dc electric field $\mathbf{E}_x = (E_1, 0, 0)$ is applied along the (x)-direction, and an external static magnetic field $\mathbf{B} = (0, 0, B)$ is applied along the (z)-axis to induce electronic transport. Then, the Hamiltonian for a single electron is given by [8, 9]

$$H_e = -\frac{(\mathbf{p} + e\mathbf{A}_B)^2}{2m_e} + \mathcal{V}(z) + eE_1x\,, \tag{2}$$

here, e is the charge, **p** is its momentum operator, the vector potential is chosen in the Landau gauge as $\mathbf{A}_B = (0, Bx, 0)$.

The electron's stationary states in the infinite semi-parabolic asymmetric quantum wells are obtained by solving the time-independent Schrödinger equation [8-10]

$$H_e\psi_{n,N,\mathbf{k}_y}^{ISPQW}(\mathbf{r}) = \varepsilon_{n,N,\mathbf{k}_y}^{ISPQW}\,\psi_{n,N,\mathbf{k}_y}^{ISPQW}(\mathbf{r}) \tag{3}$$

Through subsequent analytical steps, the resulting wave function and its corresponding energy eigenvalues are expressed as

$$\psi_{n,N,\mathbf{k}_y}^{ISPQW}(\mathbf{r}) = \frac{\exp(i\mathbf{k}_y y)}{\sqrt{L_y}}\,\varphi_N(x - x_0)\varphi_n(z) \tag{4}$$

$$\varepsilon_{N,n,\mathbf{k}_y}^{ISPQW} = \hbar\omega_c\left(N + \frac{1}{2}\right) + \hbar\omega_z\left(2n + \frac{3}{2}\right) + \hbar v_d k_y - \frac{1}{2}m_e v_d^2 \tag{5}$$

where N and n are the Landau level index and subband quantum numbers, respectively; L_y and $\mathbf{k}_y$ are the normalized length and the electron wave vector in the y direction, respectively; $\upsilon_d = \frac{E_1}{B}$ is the drift velocity, $\omega_c = \frac{eB}{m_e}$ is the cyclotron frequency; The harmonic oscillator wave functions φ_N are centered at $x_0 = -\ell_c^2\left(k_y - \frac{m_e\upsilon_d}{\hbar}\right)$; The function $\varphi_n(z)$ governs the quantized motion along the confinement direction z

$$\varphi_n(z) = \sqrt{\frac{2n!}{\ell_z^3\Gamma\left(n + \frac{3}{2}\right)}}\exp\left(-\frac{z^2}{2\ell_z^2}\right) zL_n^{\frac{1}{2}}\left(\frac{z^2}{\ell_z^2}\right) \tag{6}$$

$$\varphi_N(x - x_0) = \sqrt{\frac{1}{2^N N!\,\ell_c\sqrt{\pi}}}\exp\left(-\frac{(x - x_0)^2}{2\ell_c^2}\right) H_N\left(\frac{x - x_0}{\ell_c}\right) \tag{7}$$

here, $\ell_z = \sqrt{\frac{\hbar}{m_e\omega_z}}$ and $\ell_c = \sqrt{\frac{\hbar}{m_e\omega_c}}$ are the length of confinement along z-direction and the magnetic length, respectively; $\Gamma(x)$, L_n^k, and $H_N(x)$ are the Gamma functions, associated Laguerre polynomials, and Hermite polynomials of order N.

2.2. The Hamiltonian of an Electron-phonon System in the Infinite Semi-Parabolic Asymmetric Quantum Well for the Electron-Acoustic Phonon Scattering

The GaAs/AlGaAs ISPQW specimen is subjected to an intense electromagnetic wave with the electric field $\mathbf{E}(t) = (0, E_0\sin\Omega t, 0)$ applied along the y-axis, where E_0 and Ω represent the amplitude and frequency, respectively. A static dc electric field $\mathbf{E}_x = (E_1, 0, 0)$ is directed along the x-axis, while the magnetic field $\mathbf{B} = (0, 0, B)$ is oriented along the z-axis, as shown in Fig. (1)

The Hamiltonian describing the electron–acoustic phonon interaction in the ISPQW takes the form [10]

$$\begin{aligned}
H^{ISPQW} &= \sum_{N,n,\mathbf{k}_y} \varepsilon^{ISPQW}_{N,n,\mathbf{k}_y}\left(\mathbf{k}_y - \frac{e}{\hbar c}\mathbf{A}(t)\right) a^{+}_{N,n,\mathbf{k}_y} a_{N,n,\mathbf{k}_y} + \sum_{\mathbf{q}} \hbar\,\omega_{\mathbf{q}} b^{+}_{\mathbf{q}} b_{\mathbf{q}} + \\
&+ \sum_{N,n,\mathbf{k}_y} \sum_{N',n',\mathbf{q}} \mathcal{C}^{AP}_{\mathbf{q}} \mathcal{J}^{ISPQW}_{n,n'}(q_z) \mathcal{J}^{ISPQW}_{N,N'}(\mathbf{q}_\perp)\, a^{+}_{N',n',\mathbf{k}_y+\mathbf{q}} a_{N,n,\mathbf{k}_y}\left(b_{\mathbf{q}} + b^{+}_{-\mathbf{q}}\right) \\
&+ \sum_{N,n,\mathbf{k}_y} \varphi(\mathbf{q}) a^{+}_{N',n',\mathbf{k}_y+\mathbf{q}} a_{N,n,\mathbf{k}_y}\,, \qquad (8)
\end{aligned}$$

here, the quantum states of the electron before and after scattering are labeled by the numbers $(n, N, \mathbf{k}_y)$ and $(n, N, \mathbf{k}_y + \mathbf{q})$, respectively. The electron creation and annihilation processes are described by the operators $a^{+}_{N,n,\mathbf{k}_y}$ and $a_{N,n,\mathbf{k}_y}$, while $b^{+}_{\mathbf{q}}$ and $b_{\mathbf{q}}$ denote the corresponding creation and annihilation operators for phonons. The phonon energy is represented by $\hbar\omega_{\mathbf{q}}$. The intense EMW is introduced through the vector potential $\mathbf{A}(t) = \left(0, \frac{-E_0\cos(\Omega t)}{\Omega}, 0\right)$; $\varphi(\mathbf{q}) = (2\pi i)^3\left(e\mathbf{E} + \frac{\varepsilon - \varepsilon_F}{T}\nabla T + \omega_c[\mathbf{q}, \mathbf{h}]\right)\frac{\partial}{\partial q}\delta(\mathbf{q})$ represents the effective scalar potential of the system; the phonon wave vector $\mathbf{q} = (\mathbf{q}_\perp, \mathbf{q}_z)$, with $\mathbf{q}_z$ denoting the component along the confinement direction and $\mathbf{q}_\perp$ the in-plane component. Here, ε and ε_F correspond to the electron energy and the Fermi energy, $\hbar$ is the reduced Planck constant, and $c = 3 \times 10^8$m/s is the speed of light. The electron–acoustic phonon interaction constant is expressed as $\left|\mathcal{C}^{AP}_{\mathbf{q}}\right|^2 = \frac{\hbar\mathcal{D}^2 q}{2\rho v_s V_0}$ where $\mathcal{D}$ is the acoustic deformation potential, ρ represents the crystal mass density, v_s is the sound velocity, and $V_0 = L_x L_y L$ corresponds to the normalization volume of the quantum well structure. The factor $\mathcal{J}^{ISPQW}_{n,n'}(q_z)$ denotes the electron form factor, which originates from the effect of the confinement potential,

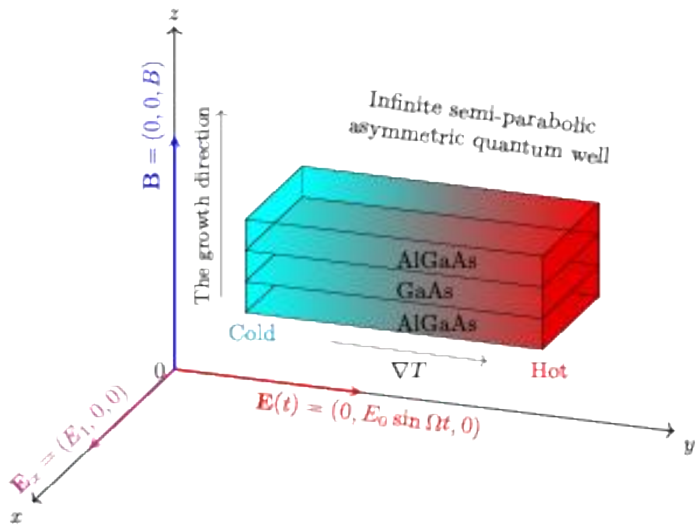

Figure 1. Schematic of the GaAs/AlGaAs infinite semi-parabolic asymmetric quantum well under external fields. The system is grown along the z-axis with $\mathbf{B} \parallel z$, subjected to a dc electric field $\mathbf{E}_x \parallel x$ and an intense EMW with $\mathbf{E}(t) \parallel y$. A temperature gradient $\nabla T \parallel y$ is also introduced, forming the basis for the Ettingshausen effect in the ISPQW structure.

$$\mathcal{I}_{n,n'}^{\mathrm{ISPQW}}(q_z) = \langle \varphi_n(z) | e^{\pm i q_z z} | \varphi_{n'}(z) \rangle , \tag{9}$$

the magnetic form factor in an ISPQW is given by

$$\begin{aligned} \mathcal{J}_{N,N'}^{\mathrm{ISPQW}}(q_\perp) &= \left| \langle \varphi_N(x - x_0) | e^{\pm i q_x x} | \varphi_{N'}(x - x_0) \rangle \right|^2 \\ &= \frac{N! \exp\left(-\frac{q_\perp^2 \ell_c^2}{2}\right)}{N'!} \left(\frac{q_\perp^2 \ell_c^2}{2}\right)^{N'-N} L_N^{N'-N}\left(\frac{q_\perp^2 \ell_c^2}{2}\right), \end{aligned} \tag{10}$$

The quantum kinetic equation describing the electron distribution function,

$$\frac{\partial f_{N,n,\mathbf{k}_y}(t)}{\partial t} = -\frac{i}{\hbar} \left\langle \left[a_{N,n,\mathbf{k}_y}^{+} a_{N,n,\mathbf{k}_y}, H \right] \right\rangle_t , \tag{11}$$

with $\partial f_{N,n,\mathbf{k}_y}(t) = \langle a_{N,n,\mathbf{k}_y}^{+} a_{N,n,\mathbf{k}_y} \rangle_t$.

By inserting the Hamiltonian given in Eq. (8) into Eq. (11) and applying the corresponding operator algebraic manipulations, one obtains

$$\begin{aligned} &\frac{\partial f_{N,n,\mathbf{k}_y}}{\partial t} + \frac{1}{\hbar}\left(\mathbf{F} + \omega_c[\mathbf{k}_y, \mathbf{h}]\right)\frac{\partial f_{N,n,\mathbf{k}_y}}{\partial \mathbf{k}_y} = \\ &= -\frac{2\pi}{\hbar} \sum_{N,n,N',n',\mathbf{q}} \left|C_{\mathbf{q}}^{\mathrm{AP}}\right|^2 \left|\mathcal{I}_{n,n'}^{\mathrm{ISPQW}}\right|^2 \left|\mathcal{J}_{N,N'}^{\mathrm{ISPQW}}\right|^2 \sum_{\ell=-\infty}^{+\infty} J_s^2\left(\Lambda^{\mathrm{LDP}} \mathbf{q}_y\right)\left(2\mathcal{N}_q + 1\right) \\ &\times \Big\{ \left[f_{N',n',\mathbf{k}_y+\mathbf{q}_y}(\mathcal{N}_q + 1) - f_{N,n,\mathbf{k}_y}\mathcal{N}_q \right] \delta\left(\varepsilon_{N',n',\mathbf{k}_y+\mathbf{q}_y}^{\mathrm{ISPQW}} - \varepsilon_{N,n,\mathbf{k}_y}^{\mathrm{ISPQW}} - \hbar\omega_{\mathbf{q}} - \ell\hbar\Omega \right) \\ &+ \left[f_{N',n',\mathbf{k}_y-\mathbf{q}_y}\mathcal{N}_q - f_{N,n,\mathbf{k}_y}(\mathcal{N}_q + 1) \right] \delta\left(\varepsilon_{N',n',\mathbf{k}_y-\mathbf{q}_y}^{\mathrm{ISPQW}} - \varepsilon_{N,n,\mathbf{k}_y}^{\mathrm{ISPQW}} + \hbar\omega_{\mathbf{q}} - \ell\hbar\Omega \right) \Big\} , \end{aligned} \tag{12}$$

where $\mathbf{F} = e\mathbf{E}_x + \frac{\varepsilon - \varepsilon_F}{T} \nabla T$; $J_\ell(x)$ denotes the Bessel function of order ℓ with argument x, and $\Lambda^{LDP} = \frac{eE_0}{m_e \Omega^2}$ denotes the laser dressing parameter; Ω corresponds to the frequency of the intense EMW. In addition, $\delta(x)$ is the Dirac delta function, and $\mathcal{N}_q$ stands for the equilibrium phonon distribution, described by the Bose–Einstein statistics.

Next, we multiply both sides of Eq. (12) by $\frac{e\hbar}{m_e}\mathbf{k}_y \delta\left(\varepsilon - \varepsilon_{N,n,\mathbf{k}_y}^{\mathrm{ISPQW}}\right)$ and subsequently perform the summation over n, N, and $\mathbf{k}_y$. For clarity, we restrict the analysis to one-photon absorption and emission processes, which reduces the order of the Bessel function in Eq. (12) to $\ell = -1, 0, 1$. Moreover, if the electron–acoustic phonon scattering is assumed to be elastic, the corresponding acoustic phonon energy in Eq. (12) can be neglected [11]. After these considerations and straightforward algebra, Eq. (12) takes the form

$$\frac{\boldsymbol{\mathcal{R}}(\varepsilon)}{\tau(\varepsilon)} + \omega_c[\mathbf{h}, \mathcal{R}(\varepsilon)] = \boldsymbol{\mathcal{Q}}(\varepsilon) + \boldsymbol{\mathcal{S}}(\varepsilon) , \tag{13}$$

here, $\tau(\varepsilon)$ denotes the relaxation time as a function of the carrier energy ε, while $\mathbf{h} = \mathbf{B}/B$ represents the unit vector along the magnetic field direction. The quantity $\mathcal{R}(\varepsilon)$ corresponds to the partial current density vector.

$$\boldsymbol{\mathcal{Q}}(\varepsilon) = -\frac{e\hbar}{m_e} \sum_{N,n,\mathbf{k}_y} \mathbf{k}_y \left(\mathbf{F}, \frac{\partial f_{N,n,\mathbf{k}_y}}{\partial \mathbf{k}_y} \right) \delta\left(\varepsilon - \varepsilon_{N,n,\mathbf{k}_y}^{\mathrm{ISPQW}} \right) \tag{14}$$

$$\begin{aligned}\boldsymbol{\mathcal{S}}(\varepsilon) &= \frac{2\pi e}{m_e}\sum_{N',n'}\sum_{N,n}\sum_{\mathbf{k}_y,\mathbf{q}}\left|C_{\mathbf{q}}^{AP}\right|^2\left|\mathcal{I}_{n,n'}^{ISPQW}\right|^2\left|\mathcal{J}_{N,N'}^{ISPQW}\right|^2\mathcal{N}_q\mathbf{k}_y\delta\left(\varepsilon-\varepsilon_{N,n,\mathbf{k}_y}^{ISPQW}\right)\times\\
&\times\Bigg\{\left(f_{N',n',\mathbf{k}_y+\mathbf{q}}-f_{N',n',\mathbf{k}_y}\right)\Bigg[\left(1-\frac{\left(\Lambda^{LBP}\right)^2\mathbf{q}_y^2}{2}\right)\delta\left(\varepsilon_{N',n',\mathbf{k}_y+\mathbf{q}}^{ISPQW}-\varepsilon_{N,n,\mathbf{k}_y}^{ISPQW}\right)+\\
&+\frac{\left(\Lambda^{LBP}\right)^2\mathbf{q}_y^2}{4}\delta\left(\varepsilon_{N',n',\mathbf{k}_y+\mathbf{q}}^{ISPQW}-\varepsilon_{N,n,\mathbf{k}_y}^{ISPQW}+\hbar\Omega\right)+\\
&+\frac{\left(\Lambda^{LBP}\right)^2\mathbf{q}_y^2}{4}\delta\left(\varepsilon_{N',n',\mathbf{k}_y+\mathbf{q}}^{ISPQW}-\varepsilon_{N,n,\mathbf{k}_y}^{ISPQW}-\hbar\Omega\right)\Bigg]+\\
&\Bigg\{\left(f_{N',n',\mathbf{k}_y-\mathbf{q}}-f_{N',n',\mathbf{k}_y}\right)\Bigg[\left(1-\frac{\left(\Lambda^{LBP}\right)^2\mathbf{q}_y^2}{2}\right)\delta\left(\varepsilon_{N',n',\mathbf{k}_y-\mathbf{q}}^{ISPQW}-\varepsilon_{N,n,\mathbf{k}_y}^{ISPQW}\right)+\\
&+\frac{\left(\Lambda^{LBP}\right)^2\mathbf{q}_y^2}{4}\delta\left(\varepsilon_{N',n',\mathbf{k}_y-\mathbf{q}}^{ISPQW}-\varepsilon_{N,n,\mathbf{k}_y}^{ISPQW}+\hbar\Omega\right)+\\
&+\frac{\left(\Lambda^{LBP}\right)^2\mathbf{q}_y^2}{4}\delta\left(\varepsilon_{N',n',\mathbf{k}_y-\mathbf{q}}^{ISPQW}-\varepsilon_{N,n,\mathbf{k}_y}^{ISPQW}-\hbar\Omega\right)\Bigg]\Bigg\}.\end{aligned}\tag{15}$$

Solving Eq. (13), we have

$$\begin{aligned}\boldsymbol{\mathcal{R}}(\varepsilon) &= \frac{\tau(\varepsilon)}{1+\omega_c^2\tau^2(\varepsilon)}\{\boldsymbol{\mathcal{Q}}(\varepsilon)+\boldsymbol{\mathcal{S}}(\varepsilon)-\omega_c\tau(\varepsilon)[\boldsymbol{\mathcal{Q}}(\varepsilon)+\boldsymbol{\mathcal{S}}(\varepsilon)]+\\
&+\omega_c^2\tau^2(\varepsilon)\mathbf{h}\big(\mathbf{h},\boldsymbol{\mathcal{Q}}(\varepsilon)+\boldsymbol{\mathcal{S}}(\varepsilon)\big)\}\end{aligned}\tag{16}$$

The expression for the total current density is calculated as follows

$$\mathbf{j}(t)=\int_0^{+\infty}\boldsymbol{\mathcal{R}}(\varepsilon)d\varepsilon=\frac{e\hbar}{m_e}\int_0^{+\infty}\sum_{N,n,\mathbf{k}_y}\mathbf{k}_y f_{N,n,\mathbf{k}_y}(t)\delta\left(\varepsilon-\varepsilon_{N,n,\mathbf{k}_y}^{ISPQW}\right)d\varepsilon.\tag{17}$$

2.3. The analytical Expressions for Thermal Conductivity Tensors, Electric Conductivity Tensors, and the Ettingshausen Coefficient

We have the general formula of the EC in ISPQW for the case of electron-acoustic phonon scattering as below [12]

$$EC^{ISPQW}=\frac{1}{B}\cdot\frac{\sigma_{xx}^{ISPQW}.\gamma_{xy}^{ISPQW}-\sigma_{xy}^{ISPQW}.\gamma_{xx}^{ISPQW}}{\sigma_{xx}^{ISPQW}.\left[\beta_{xx}^{ISPQW}.\gamma_{xx}^{ISPQW}-\sigma_{xx}^{ISPQW}.\left(\xi_{xx}^{ISPQW}-K_L\right)\right]},\tag{18}$$

In this context, K_L denotes the lattice thermal constant, whose magnitude is sufficiently small to be neglected. The quantity σ_{xx}^{ISPQW}, σ_{xy}^{ISPQW} represent the electrical conductivity tensors, while β_{xx}^{ISPQW} corresponds to the thermoelectric tensor. Similarly, γ_{xx}^{ISPQW}, γ_{xy}^{ISPQW} are the dynamic tensors associated with the electric field $\mathbf{E}_m$, and ξ_{xx}^{ISPQW} is the dynamic tensor related to the thermal gradient ∇T_m.

We derive the analytical forms of these tensors as follows. In Eq. (17), the expression for the total current density $\mathbf{j}$ has been obtained. Based on this relation, the conductivity tensor σ_{im}^{ISPQW} and the thermoelectric tensor β_{im}^{ISPQW} can be extracted using the thermoelectric transport equation [13].

$$\mathbf{j}=\sigma_{im}^{ISPQW}\mathbf{E}_m+\beta_{im}^{ISPQW}\boldsymbol{\nabla}\mathbf{T}_m\,.\tag{19}$$

Next, in order to derive the expressions for the remaining tensors $\gamma_{\mathrm{im}}^{\mathrm{ISPQW}}$ and $\xi_{\mathrm{im}}^{\mathrm{ISPQW}}$, we make use of the thermal flux density relation, given by [13].

$$\boldsymbol{Q}(\varepsilon) = -\frac{1}{\mathrm{e}}\int_0^{+\infty}(\varepsilon-\varepsilon_{\mathrm{F}})\boldsymbol{\mathcal{R}}(\varepsilon)\mathrm{d}\varepsilon = \gamma_{\mathrm{im}}^{\mathrm{ISPQW}}\mathbf{E}_{\mathrm{m}} + \xi_{\mathrm{im}}^{\mathrm{ISPQW}}\nabla\mathbf{T}_{\mathrm{m}}. \tag{20}$$

The analytical forms of the kinetic tensors are given by

$$\begin{aligned}\sigma_{\mathrm{xx}}^{\mathrm{ISPQW}} &= \frac{\tau(\varepsilon_{\mathrm{F}})(1-\omega_c\tau)}{1+\omega_c^2\tau^2(\varepsilon_{\mathrm{F}})}\mathcal{A}_0 + [\mathcal{Y}_1+\mathcal{Y}_2]\frac{\mathrm{e}\,\tau^2\mathcal{P}}{\mathrm{m_e}[1+\omega_c^2\tau^2\mathcal{P}]^2} + \\ &+\mathcal{X}_1\frac{\mathrm{e}\,\tau^2(\mathcal{P}-\hbar\Omega)}{\mathrm{m_e}[1+\omega_c^2\tau^2(\mathcal{P}-\hbar\Omega)]^2} + \mathcal{X}_2\frac{\mathrm{e}\,\tau^2(\mathcal{P}+\hbar\Omega)}{\mathrm{m_e}[1+\omega_c^2\tau^2(\mathcal{P}+\hbar\Omega)]^2}\end{aligned} \tag{21}$$

$$\begin{aligned}\sigma_{\mathrm{xy}}^{\mathrm{ISPQW}} &= \frac{\tau(\varepsilon_{\mathrm{F}})(1-\omega_c\tau)}{1+\omega_c^2\tau^2(\varepsilon_{\mathrm{F}})}\mathcal{A}_0 + [\mathcal{Y}_1+\mathcal{Y}_2]\frac{\mathrm{e}\,\tau^2\mathcal{P}(\omega_c\tau\mathcal{P})^2}{\mathrm{m_e}[1+\omega_c^2\tau^2\mathcal{P}]^2} + \\ &+\mathcal{X}_1\frac{\mathrm{e}\,\tau^2(\mathcal{P}-\hbar\Omega)\mathcal{P}_1^2}{\mathrm{m_e}[1+\omega_c^2\tau^2(\mathcal{P}-\hbar\Omega)]^2} + \mathcal{X}_2\frac{\mathrm{e}\,\tau^2(\mathcal{P}+\hbar\Omega)\mathcal{P}_2^2}{\mathrm{m_e}[1+\omega_c^2\tau^2(\mathcal{P}+\hbar\Omega)]^2}\end{aligned} \tag{22}$$

$$\begin{aligned}\beta_{\mathrm{xx}}^{\mathrm{ISPQW}} &= -(\mathcal{Y}_1+\mathcal{Y}_2)(\mathcal{P}-\varepsilon_{\mathrm{F}})\frac{\mathrm{e}\tau^2\mathcal{P}}{\mathrm{m_e T}[1+\omega_c^2\tau^2\mathcal{P}]^2} - \\ &-\mathcal{X}_1(\mathcal{P}-\hbar\Omega-\varepsilon_{\mathrm{F}})\frac{\mathrm{e}\,\tau^2(\mathcal{P}-\hbar\Omega)}{\mathrm{m_e T}[1+\omega_c^2\tau^2(\mathcal{P}-\hbar\Omega)]^2} - \\ &-\mathcal{X}_2(\mathcal{P}+\hbar\Omega-\varepsilon_{\mathrm{F}})\frac{\mathrm{e}\,\tau^2(\mathcal{P}+\hbar\Omega)}{\mathrm{m_e T}[1+\omega_c^2\tau^2(\mathcal{P}+\hbar\Omega)]^2},\end{aligned} \tag{23}$$

$$\begin{aligned}\gamma_{\mathrm{xx}}^{\mathrm{ISPQW}} &= (\mathcal{Y}_1+\mathcal{Y}_2)(\mathcal{P}-\varepsilon_{\mathrm{F}})\frac{\mathrm{e}\tau^2\mathcal{P}}{\mathrm{m_e}[1+\omega_c^2\tau^2\mathcal{P}]^2} + \\ &+\mathcal{X}_1(\mathcal{P}-\hbar\Omega-\varepsilon_{\mathrm{F}})\frac{\mathrm{e}\,\tau^2(\mathcal{P}-\hbar\Omega)}{\mathrm{m_e}[1+\omega_c^2\tau^2(\mathcal{P}-\hbar\Omega)]^2} + \\ &+\mathcal{X}_2(\mathcal{P}+\hbar\Omega-\varepsilon_{\mathrm{F}})\frac{\mathrm{e}\,\tau^2(\mathcal{P}+\hbar\Omega)}{\mathrm{m_e}[1+\omega_c^2\tau^2(\mathcal{P}+\hbar\Omega)]^2},\end{aligned} \tag{24}$$

$$\begin{aligned}\gamma_{\mathrm{xy}}^{\mathrm{ISPQW}} &= (\mathcal{Y}_1+\mathcal{Y}_2)(\mathcal{P}-\varepsilon_{\mathrm{F}})\frac{\mathrm{e}\tau^2\mathcal{P}(\omega_c\tau\mathcal{P})^2}{\mathrm{m_e}[1+\omega_c^2\tau^2\mathcal{P}]^2} + \\ &+\mathcal{X}_1(\mathcal{P}-\hbar\Omega-\varepsilon_{\mathrm{F}})\frac{\mathrm{e}\,\tau^2(\mathcal{P}-\hbar\Omega)\mathcal{P}_1^2}{\mathrm{m_e}[1+\omega_c^2\tau^2(\mathcal{P}-\hbar\Omega)]^2} + \\ &+\mathcal{X}_2(\mathcal{P}+\hbar\Omega-\varepsilon_{\mathrm{F}})\frac{\mathrm{e}\,\tau^2(\mathcal{P}+\hbar\Omega)\mathcal{P}_2^2}{\mathrm{m_e}[1+\omega_c^2\tau^2(\mathcal{P}+\hbar\Omega)]^2},\end{aligned} \tag{25}$$

$$\begin{aligned}\xi_{\mathrm{xx}}^{\mathrm{ISPQW}} &= -\left(\mathcal{Y}_1+\mathcal{Y}_2\right)(\mathcal{P}-\varepsilon_{\mathrm{F}})^2\frac{\mathrm{e}\tau^2\mathcal{P}}{\mathrm{m_e T}[1+\omega_c^2\tau^2\mathcal{P}]^2} - \\ &-\mathcal{X}_1(\mathcal{P}-\hbar\Omega-\varepsilon_{\mathrm{F}})^2\frac{\mathrm{e}\,\tau^2(\mathcal{P}-\hbar\Omega)}{\mathrm{m_e T}[1+\omega_c^2\tau^2(\mathcal{P}-\hbar\Omega)]^2} - \\ &-\mathcal{X}_2(\mathcal{P}+\hbar\Omega-\varepsilon_{\mathrm{F}})^2\frac{\mathrm{e}\,\tau^2(\mathcal{P}+\hbar\Omega)}{\mathrm{m_e T}[1+\omega_c^2\tau^2(\mathcal{P}+\hbar\Omega)]^2},\end{aligned} \tag{24}$$

Where,

$$\mathcal{A}_0 = \frac{eL_y}{2\pi m_e \hbar^2 v_d}\varepsilon^{ISPQW}_{n,N,\mathbf{k}_y}; \quad \mathcal{P} = \varepsilon^{ISPQW}_{n',N',\mathbf{k}_y} - \varepsilon^{ISPQW}_{n,N,\mathbf{k}_y} - eE_1\lambda$$

$$\lambda = \left(\sqrt{N+\frac{1}{2}} + \sqrt{N+\frac{3}{2}}\right)\frac{\ell_c}{2}; \quad \mathcal{P}_1 = \omega_c\tau(\mathcal{P}-\hbar\Omega); \quad \mathcal{P}_2 = \omega_c\tau(\mathcal{P}+\hbar\Omega)$$

$$\mathcal{Y}_1 = \mathcal{G}\left(1 - \frac{\left(\Lambda^{LDP}\right)^2\lambda^2}{2\ell_c^2}\right)\left[1 + 2\sum_{l=1}^{\infty}(-1)^l e^{\left(-\frac{2\pi l\kappa}{\hbar\omega_c}\right)}\cos(2\pi l\varrho_1)\right]$$

$$\mathcal{Y}_2 = \mathcal{G}\frac{\left(\Lambda^{LDP}\right)^2\lambda^2}{4\ell_c^2}\left[1 + 2\sum_{l=1}^{\infty}(-1)^l e^{\left(-\frac{2\pi l\kappa}{\hbar\omega_c}\right)}\cos(2\pi l\varrho_1)\right]$$

$$\mathcal{X}_1 = \mathcal{G}\frac{\left(\Lambda^{LDP}\right)^2\lambda^2}{4\ell_c^2}\left[1 + 2\sum_{l=1}^{\infty}(-1)^l e^{\left(-\frac{2\pi l\kappa}{\hbar\omega_c}\right)}\cos(2\pi l\varrho_2)\right]$$

$$\mathcal{X}_2 = \mathcal{G}\frac{\left(\Lambda^{LDP}\right)^2\lambda^2}{4\ell_c^2}\left[1 + 2\sum_{l=1}^{\infty}(-1)^l e^{\left(-\frac{2\pi l\kappa}{\hbar\omega_c}\right)}\cos(2\pi l\varrho_3)\right]$$

$$\varrho_1 = \frac{\varepsilon^{ISPQW}_{n,N,\mathbf{k}_y} - \varepsilon^{ISPQW}_{n',N',\mathbf{k}_y} + eE_1\lambda}{\hbar\omega_c}; \quad \varrho_2 = \frac{\varepsilon^{ISPQW}_{n,N,\mathbf{k}_y} - \varepsilon^{ISPQW}_{n',N',\mathbf{k}_y} + eE_1\lambda - \hbar\Omega}{\hbar\omega_c}$$

$$\varrho_3 = \frac{\varepsilon^{ISPQW}_{n,N,\mathbf{k}_y} - \varepsilon^{ISPQW}_{n',N',\mathbf{k}_y} + eE_1\lambda + \hbar\Omega}{\hbar\omega_c}; \quad \kappa = \frac{\hbar}{\tau};$$

$$\mathcal{G} = \frac{e\eta_0\mathcal{D}^2 m_e k_B T L_y L}{8\pi^2\hbar^4\rho v_d v_s^3}\int_{-\infty}^{+\infty}\left|\mathcal{I}^{ISPQW}_{n,n'}(q_z)\right|^2\lambda(\varepsilon^{ISPQW}_{n,N} - \varepsilon_F)\,dq_z\,,$$

with η_0 is the electron's density

By inserting the tensors into Eq. (18) the analytical form of EC^{ISPQW} is obtained.

3. Numerical Result for Semi-parabolic Quantum Wells with an Infinite Potential

To illustrate the physical significance of the obtained result, we numerically evaluate the EC coefficient for GaAs/AlGaAs heterostructures using specific material parameters [14,15]: $\varepsilon = \varepsilon_F = 50$meV , $m_e = 0.067\ m_o$ (m_o is the mass of free electron, $m_0 = 9.1 \times 10^{-31}$ kg), $\tau = 10^{-12}$ s, $\upsilon_s = 5220$ ms^{-1}, $e_0 = 1.6 \times 10^{-19}$ C, $e = 2.07e_0$, $\varepsilon_0 = 8.86 \times 10^{-12}$. In this analysis, only transitions between the lowest neighboring energy levels are taken into account, while the minor contributions from distant-state transitions are neglected. Accordingly, we restrict ourselves to electron transitions between the lowest subbands $n = 0 \rightarrow n' = 1$ and $N = 0 \rightarrow N' = 1$.

To elucidate the combined effects of the magnetic field and the external EM wave on the thermomagnetic transport, we have calculated the Ettingshausen coefficient as a function of these parameters. Fig. (2a) illustrates the results of these calculations, showing the EC as a function of the magnetic field B, under the influence of an intense EMW at three distinct frequencies. These results reveal the essential transport characteristics of the system under investigation.

The dependence of the EC on the magnetic field is characterized by two primary features. Firstly, a general underlying trend is observed, wherein the magnitude of the EC gradually decreases with increasing magnetic field strength. Superimposed on this trend is the second and more prominent feature: the presence of distinct Shubnikov-de Haas (SdH) quantum oscillations. The existence of these oscillations provides unambiguous evidence of the quantum nature of the electronic transport processes within the material. Furthermore, the frequency of the external EMW Ω, is shown to be a critical tuning parameter that profoundly modifies the EC. As Ω is increased, two concurrent effects are observed, as detailed in Fig. (2a). First, the amplitude of the quantum oscillations is significantly suppressed. A direct comparison shows that the most pronounced oscillations occur for the green curve ($\Omega = 5.0 \times 10^{13}$Hz). As the frequency increases, the amplitude is markedly reduced for the magenta curve ($\Omega = 7.5 \times 10^{13}$Hz) and is almost completely quenched for the blue dashed curve ($\Omega = 10 \times 10^{13}$Hz). Second, the overall magnitude of the EC is also diminished with increasing Ω.

Both of these phenomena can be attributed to the enhancement of photon-assisted inelastic scattering processes. The 3D surface plot in Fig. (2b) provides a comprehensive visualization of these dependencies, where the color scale maps low EC values to blue and high EC values to red. This plot confirms that the Ettingshausen coefficient is maximized in the red region, corresponding to the regime of low magnetic fields and low EM wave frequencies, while it is minimized in the blue regions.

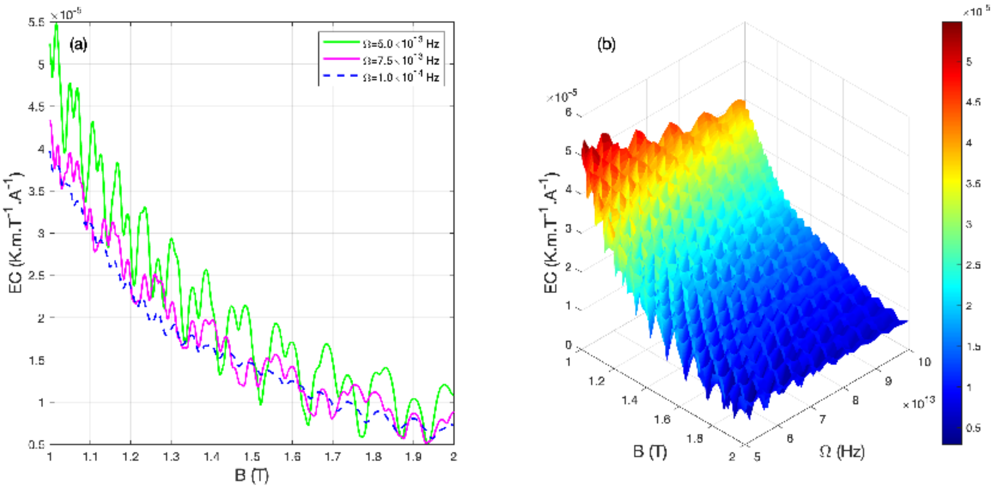

Figure 2. (a) The dependence of the EC on the magnetic field B for three different values of the intense EMW frequency Ω. (b) The dependence of the EC on the magnetic field B and intense EMW frequency Ω.

To further elucidate the factors governing the system, we investigated the role of temperature (T) on the Ettingshausen coefficient (EC), with the results presented in Fig. 3. The results reveal a profound and somewhat counter-intuitive influence of temperature on both the overall magnitude and the quantum oscillatory features of the EC. As illustrated in Fig. (3a), as the temperature is increased from T = 5K (green curve) to T = 10K (magenta curve) and T = 15K (blue dashed curve), two distinct changes are observed. In this case, an increase in temperature leads to a significant enhancement of the Shubnikov-de Haas oscillation amplitude. A visual inspection confirms that the curve at T = 15K exhibits the largest peak-to-valley contrast. Furthermore, the overall magnitude of the Ettingshausen coefficient also shows a clear positive dependence on temperature, with the T = 15K curve positioned highest.

The 3D surface plot in Fig. (3b) comprehensively reinforces these observations. The color scale, which maps low EC values to blue and high values to red, confirms that the coefficient systematically increases as the temperature rises within the investigated range. The surface plot also shows that the "ripples" corresponding to the oscillations become more prominent in the high-temperature regime, associated with the red and yellow regions. This suggests that, within the theoretical model under consideration, thermal effects appear to play an amplifying, rather than a damping, role in the quantum transport phenomena.

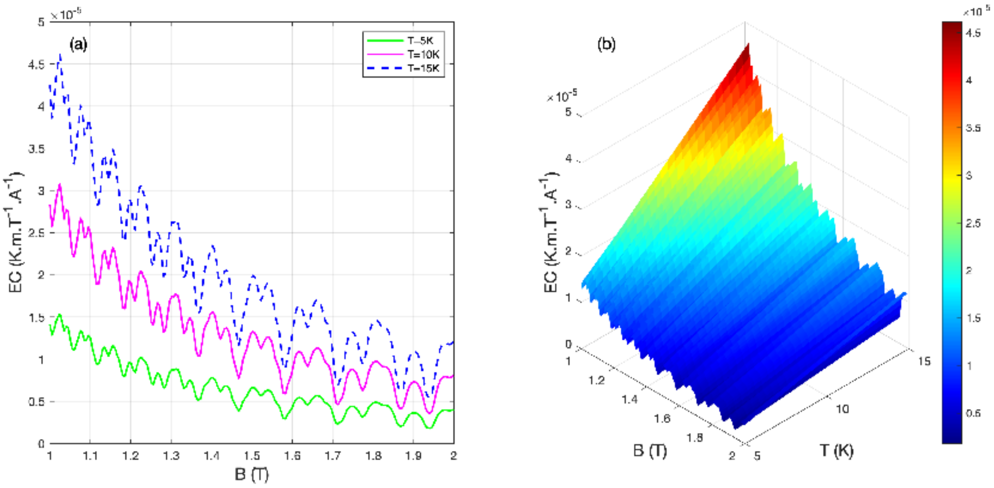

Figure 3. (a) The dependence of the EC on the magnetic field B for three different values of temperature T. (b) The dependence of the EC on the magnetic field B and temperature T.

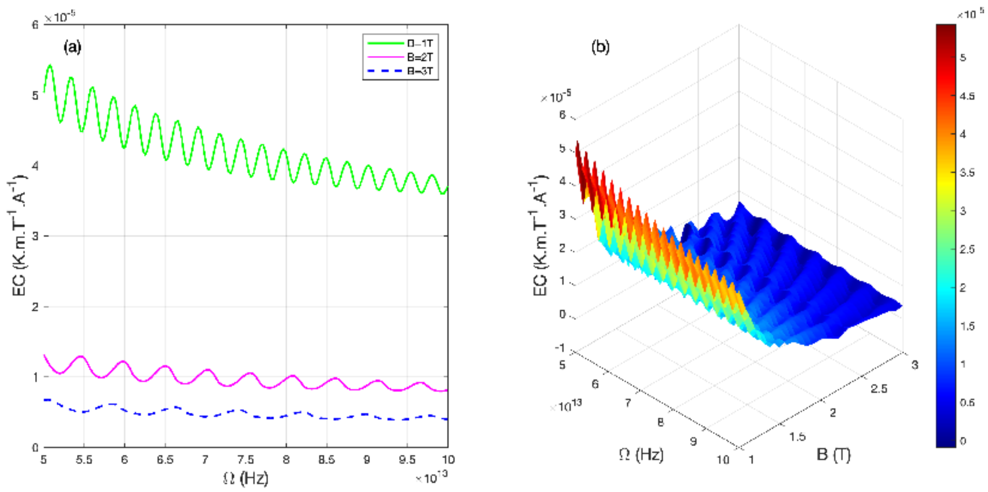

Figure 4. (a) The dependence of the EC on the intense EMW frequency Ω for three different values of the magnetic filed B. (b) The dependence of the EC on the intense EMW frequency Ω and magnetic field B.

Continuing the investigation, we now turn to the explicit dependence of the EC on the frequency of the intense EMW Ω. Fig. (4a) presents this relationship at three different, constant values of the magnetic field B. A prominent feature observed in Fig. (4a) is the overall decrease of the EC's magnitude as the frequency Ω increases. This trend is consistently observed for all magnetic fields investigated: B=1T (green curve), B=2T (magenta curve), and B=3T (blue dashed curve). Superimposed on this general reduction are periodic oscillations. It is important to note that the amplitude of these oscillations also undergoes attenuation with increasing Ω. This is most clearly visible for the B=1T curve, where the oscillations at lower frequencies are markedly more pronounced than those at higher frequencies.

The magnetic field B remains a dominant control parameter for the overall magnitude of the coefficient. As clearly shown, the EC is substantially suppressed as B is increased from 1T to 3T. The 3D plot in Fig. (4b) provides a holistic view of these behaviors, with the color scale from blue (low) to red (high) confirming that the EC is maximized in the regime of low magnetic field and low EMW frequency.

Building upon the previous analyses, we now investigate the combined influence of temperature and the EMW frequency on the EC. Fig. (5a) presents the dependence of the EC on the intense EMW frequency Ω for three different values of temperature T. The results shown in Fig. (5a) reveal several key trends. Consistent with the findings in Fig. (4), the EC exhibits a general decrease in magnitude as the frequency Ω increases for all temperatures studied, with periodic oscillations superimposed on this trend. Concurrently, temperature acts as a significant amplifying factor, causing a systematic increase in the overall magnitude of the EC as the temperature rises from T=5K (green curve) to T=10K (magenta curve) and T=15K (blue dashed curve). This confirms the anomalous temperature dependence noted in the analysis of Fig. (3), where thermal effects enhance the coefficient rather than suppressing it.

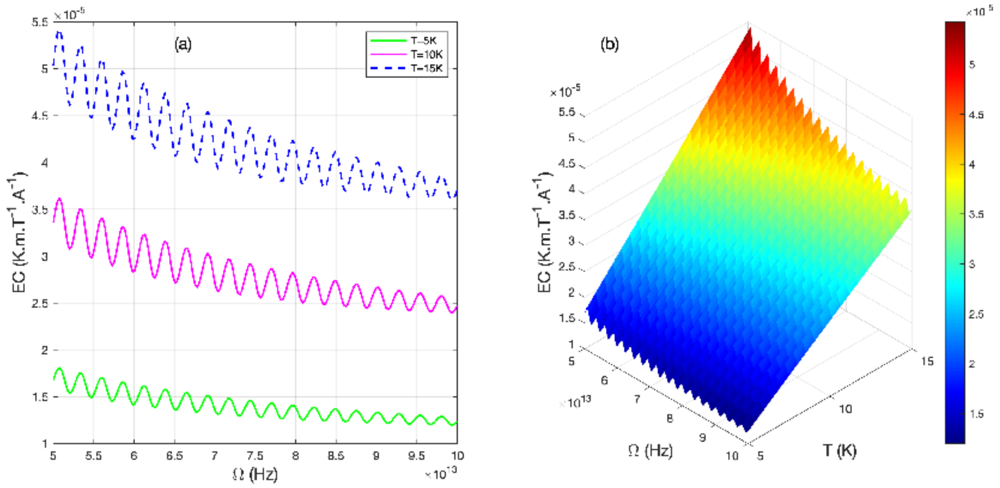

Figure 5. (a) The dependence of the EC on the intense EMW frequency Ω for three different values of the temperature T. (b) The dependence of the EC on the intense EMW frequency Ω and temperature T.

The 3D surface plot in Fig. (5b) provides a comprehensive map of these combined effects. The color scale, ranging from blue (low EC values) to red (high EC values), clearly illustrates that the EC is maximized in the regime of high temperature and low EMW frequency. This visualization encapsulates the competing influences observed: the suppressive effect of the EMW frequency and the amplifying effect of temperature.

The investigation now proceeds to examine the influence of the confinement frequency ω_z, on the EC, with the results presented in Fig. (6). A dramatically different oscillatory behavior is observed in Fig. (6a). In contrast to the relatively low-amplitude oscillations seen in previous figures, the EC now exhibits powerful oscillations with extremely large amplitudes at specific values of the confinement frequency. These high-amplitude oscillations are located at approximately $\omega_z \approx 2.3 \times 10^{13}$Hz and $\omega_z \approx 5 \times 10^{13}$Hz, suggesting a harmonic relationship. The sharp, divergent nature of these peaks indicates a strong, resonant-like enhancement of the oscillatory phenomenon. The frequency of the intense EMW Ω, continues to be a crucial modulating parameter. While the positions of the high-amplitude oscillations do not shift with Ω, their magnitudes are strongly dependent on it. The most powerful oscillations are observed for the magenta curve ($\Omega = 5.0 \times 10^{13}$ Hz). In contrast, the amplitudes are significantly suppressed for both lower ($\Omega = 1.0 \times 10^{13}$ Hz, green curve) and higher ($\Omega = 10.0 \times 10^{13}$ Hz, blue dashed curve) EMW frequencies. The 3D surface plot in Fig. (6b) provides a comprehensive visualization. The positive peaks (red colors) and negative peaks (blue color) confirm that the condition for these strong oscillations is determined by ω_z. The plot clearly shows that the intensity of these features is maximized for an intermediate range of Ω, encapsulating the modulating role of the external EMW.

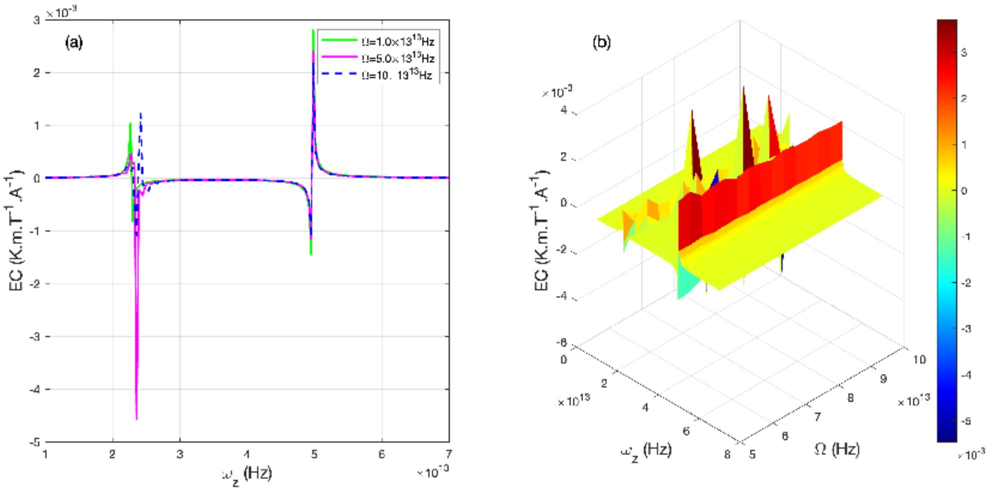

Figure 6. (a) The dependence of the EC on the confinement frequency ω_z for three different values of the intense EMW frequency Ω. (b) The dependence of the EC on the confinement frequency ω_z and intense EMW frequency Ω.

Finally, to complete the study, we analyze the dependence of the Ettingshausen coefficient (EC) on temperature T, at three constant magnetic field values. The results, presented in Fig. (7a), reveal the dominant thermal behavior of the system in this regime. A clear and consistent trend is observed in Fig. (7a). For magnetic fields of B=3T (green curve) and B=7T (blue dashed curve), the EC exhibits a nearly linear increase with temperature. However, the behavior at B=5T (magenta curve) is anomalous, showing a slight decrease. This starkly contrasts with the quantum oscillatory phenomena seen in previous figures, indicating that in this parameter space, the primary characteristic is the monotonic (or nearly monotonic) thermal response.

The magnetic field B acts as a strong, non-trivial control parameter for this thermal dependence. The rate of increase of the EC with temperature is steepest at B=3T, and significantly less so at B=7T. This confirms that a lower magnetic field leads to a stronger thermal response.The 3D surface plot in Fig. (7b) provides a comprehensive visualization of this relationship. The surface shows a complex, folded structure rather than a simple plane. The color scale, from blue (negative EC) to red (high positive EC), confirms that the coefficient generally increases with temperature, but this increase is strongly modulated by the magnetic field. The absence of fine oscillatory features underscores that, in this parameter regime, the broad temperature and magnetic field dependencies are the primary characteristics of the system's thermomagnetic response.

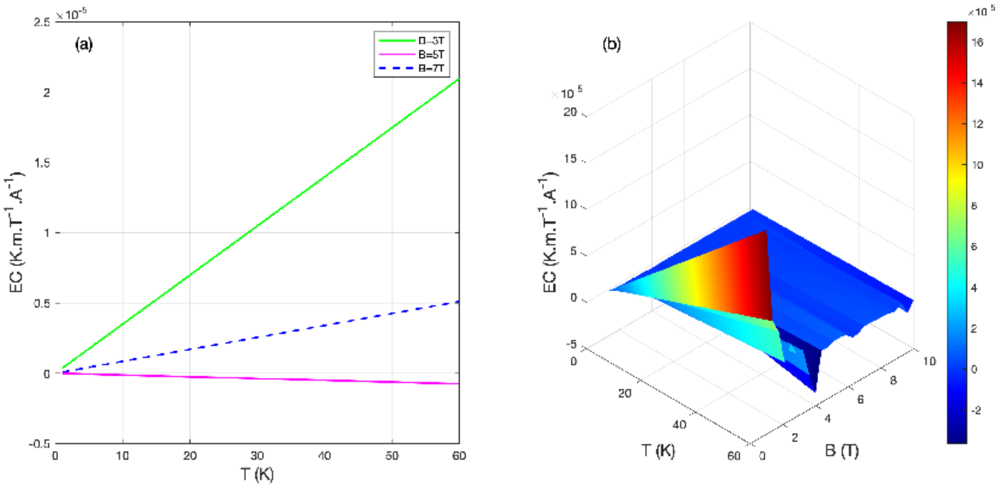

Figure 7. (a) The dependence of the EC on the temperature T for three different values of the magnetic field B. (b) The dependence of the EC on the temperature T and magnetic field B.

4. Conclusion

In this work, we have performed a comprehensive theoretical analysis of the EC in a two-dimensional system modeled by an infinite semi-parabolic asymmetric quantum well, which serves as an exemplary system for studying the effects of asymmetric confining potential on quantum thermomagnetic phenomena. By applying the quantum kinetic equation method for the electron-acoustic phonon scattering mechanism, we successfully derived analytical expressions for the EC and the associated kinetic tensors.

Our main findings, based on numerical calculations for a GaAs/AlGaAs heterostructure, have conclusively demonstrated that the transport properties of the system are profoundly influenced by both the asymmetric confinement and the external fields. Specifically, we observed distinct Shubnikov-de Haas (SdH) quantum oscillations, whose amplitudes are anomalously amplified by increasing temperature but suppressed by an increasing EMW frequency (Ω). In contrast to the conventional damping effect, the overall magnitude of the EC shows a nearly linear increase with temperature, indicating that thermal effects in this model play an amplifying rather than a dissipative role. Furthermore, variations with confinement frequency ω_z produce large-amplitude quantum oscillations, reflecting strong quantization effects arising from the asymmetric confining potential. The amplitude of these oscillations can be modulated by the EMW frequency. The magnitude of the EC systematically decreases with increasing magnetic field strength and EMW frequency, confirming the role of these parameters as effective tools for controlling the system's thermomagnetic response.

In summary, this study not only elucidates the complex thermomagnetic behaviors in asymmetric nanostructures but also highlights the potential for engineering heat transport at the quantum level. The findings on temperature-induced amplification and resonance modulation open new avenues for the future design of advanced thermoelectric components and quantum devices.

Acknowledgments

This research is financially supported by Vietnam National University, Hanoi - Grant Number QG.24.125.

References

[1] N. Q. Bau, D. T. Hang, D. T. Long, Study of the Quantum Magneto-Thermoelectric Effect in the Two-Dimensional Compositional Superlattice GaAs/AlGaAs under the Influence of an Electromagnetic Wave, Journal of the Korean Physical Society, Vol. 75, 2019, pp. 1004-1016, https://doi.org/10.3938/jkps.75.1004.

[2] F. M. Hashimzade, K. A. Hasanov, B. H. Mehdiyev, S. Cakmak, Magneto-thermoelectric Effects in Two-Dimensional Quantum Well: Role of Short-Range Potential, Physica Scripta, Vol. 81, 2010, pp. 015701.

[3] F. M. Hashimzade, Kh. A. Hasanov, B. H. Mehdiyev, Magnetothermoelectric Effects of 2D Electron Gas in Quantum Well with Parabolic Confinement Potential in-plane Magnetic Field, J. Phys.: Conf. Ser., Vol. 245, 2010, pp. 012015.

[4] A. A. Perov, P. V. Pikunov, Transverse Nernst–Ettingshausen Effect in the Two-Dimensional Electron Gas of a Doubly Periodic Semiconductor Superlattice, Semiconductors, Vol. 55, 2022, pp. 869-873.

[5] N. Q. Bau, D. T. Hang, D. M. Quang, N. T. T. Nhan, Magneto-thermoelectric Effects in Quantum Well in the Presence Of Electromagnetic Wave, VNU Journal of Science: Mathematics-Physics, Vol. 33, No. 2, 2017, pp. 1-9.

[6] C. T. V. Ba, N. Q. Bau, N. T. L. Quynh, N. D. Nam, D. T.Long, Theoretical Study of Photo-Stimulated Thermo-Magnetoelectric Effects in Two-Dimensional Compositional Superlattices Using Quantum Kinetic Equation, Journal of the Korean Physical Society, Vol. 81, 2022, pp. 757-769.

[7] M. J. Karimi, A. Keshavarz, A. Poostforush, Linear and Nonlinear Intersubband Optical Absorption of Finite and Infinite Semi-Parabolic Quantum Wells, Modern Physics Letters B, Vol. 25, No. 7, 2011, pp. 497-507, https://doi.org/10.1142/S0217984911025882.

[8] P. Vasilopoulos, M. Charbonneau, C. M. V. Vliet, Linear and Nonlinear Electrical Conduction in Quasi-Two-Dimensional Quantum Wells, Physical Review B, Vol. 35, No. 3, 1987, pp. 1334, doi.org/10.1103/PhysRevB.35.1334.

[9] N. T. Huong, N. Q. Bau, C. T. V. Ba, B. T. Dung, N. C. Toan, A. T. Tran, Theoretical Study of Magnetoresistance Oscillations in Semi-Parabolic Plus Semi-Inverse Squared Quantum Wells in the Presence of Intense Electromagnetic Waves, Phys. Scr., Vol. 100, 2024, pp. 015984.

[10] L. V. Tung and H. V. Phuc, "Nonlinear optical absorption via two-photon process in asymmetrical semi-parabolic quantum wells," Superlattices and Microstructures, vol. 89, pp. 288-295, 2016, doi: 10.1016/j.spmi.2015.11.014.

[11] P. Vasilopoulos, Magnetophonon Oscillations in Quasi-Two-Dimensional Quantum Wells, Physical Review B, Vol. 33, 1986, pp. 8587.

[12] B. V. Paranjape, J. S. Levinger, Theory of the Ettingshausen Effect in Semiconductors, Phys. Rev., Vol. 120, 1960, pp. 437.

[13] N. Q. Bau, D. T. Hang, D. T. Long, Study of the Quantum Magneto-thermoelectric Effect in the Two-Dimensional Compositional Superlattice GaAs/AlGaAs under the Influence of an Electromagnetic Wave by Using The Quantum Kinetic Equation, J. Korean Phys. Soc., Vol. 75, 2019, pp. 1004-1016.

[14] B. K. Ridley, Quantum Processes in Semiconductors, 5th ed. Oxford, UK: Oxford University Press, 2013. doi:10.1093/acprof:oso/9780199677214.001.0001.

[15] J. Singh, Physics of Semiconductors and Their Heterostructures, Pub. McGraw-Hill, Add. Singapore, 1993, https://books.google.com.vn/books?id=vUWRzQEACAAJ.